

https://doi.org/10.1070/QEL16903

Measuring optical properties of human liver between 400 and 1000 nm

I. Carneiro, S. Carvalho, R. Henrique, L. Oliveira, V.V. Tuchin

Abstract. **Laser diagnostics and treatment procedures are commonly performed for visible and near-IR wavelengths. The knowledge of the wavelength dependences for the optical properties of various biological tissues in this spectral range is useful for clinical applications. Since the optical properties of human liver have been previously known only for near-IR wavelengths, the aim is to estimate their wavelength dependences between 400 and 1000 nm. Using spectral measurements from liver samples in this range, we determine their optical properties with the inverse adding-doubling method. The obtained results indicate the presence of bile, oxyhaemoglobin and deoxyhaemoglobin in human liver. The combination of these biological components results in strong absorption for wavelengths between 400 and 600 nm, with peaks at unusual wavelengths. For wavelengths above 600 nm, the wavelength dependences for all optical properties present the typical behavior, but strong and shifted absorption observed for wavelengths below 600 nm has been previously unknown and can be useful for clinical procedures with lasers working in this range.**

Keywords: *human liver, lasers, inverse adding-doubling, absorption coefficient, scattering coefficient, scattering anisotropy factor, light penetration depth.*

1. Introduction and theoretical background

Noninvasive diagnosis or treatment procedures are made using lasers at various wavelengths. Considering the wavelength range from 400 to 1000 nm, many different lasers are used in diagnostic and therapeutic techniques such as photodynamic therapy [1], interstitial thermal therapy [1] or plasmonic-resonant photothermal therapy [1–2]. The quantification of tissue's optical properties in such a wide wavelength range is therefore important. Mapping the optical properties of biological tissues is also highly important for the development and improvement of biophotonics techniques. Since the optical properties of tissues are their optical identity card, their knowledge is necessary so that light propagation models can be created and adjusted from tissue to tissue [3–5]. With the exception of the refractive index (RI), which can be measured directly, tissue's optical properties must be estimated from optical measurements. Indirect estimation methods, based on common optical measurements like collimated transmittance (T_c), total transmittance (T_t) and total reflectance (R_t) are inexpensive and fast and provide a good alternative to obtain the optical properties of biological materials with considerable precision. The most known estimation methods are inverse Monte Carlo (IMC) [6] and inverse adding-doubling (IAD) [7]. The codes of these estimation methods were developed in the 1990s and are still today the most accurate codes used for estimating the optical properties. In each of these estimation methods, a large number of photons are used to interact with a tissue with a preestablished set of optical properties. Based on these properties and using the radiative transfer theory, some measureable quantities, like T_t, R_t and T_c, are estimated [8]. Such estimated quantities are compared with experimental measurements and if the difference between generated and experimental data is too high, the optical properties considered in the simulation are corrected to simulate again. These methods are iterative and they run until a minimum difference is obtained between generated and experimental data [9]. According to the literature [10], the IMC method is more accurate than the IAD, but simulations with the IAD method are faster and quite precise [8, 10]. Both the IAD and the direct MC codes are kept available online at the website of the Oregon Medical Laser Center [11]. The IMC code is not available, but it can be developed from the direct MC code. The estimation of the optical properties with these codes is made for individual wavelengths, meaning that to obtain the wavelength dependences for the optical properties of a tissue within a spectral range, it is necessary to perform several simulations – one for each wavelength.

The interest in the wavelength dependences of tissue's optical properties is big and some recent papers present such data for tissues like: skull [12], skin, subcutaneous and mucous tissues [13], breast [14], colorectal tissues [3, 8, 9], forearm, calf and head tissues [15], peritoneal tissues [10] or stomach mucosa [16].

I. Carneiro, S. Carvalho Portuguese Oncology Institute of Porto, Department of Pathology and Cancer Biology and Epigenetics Group-Research Centre, Rua Dr. António Bernardino de Almeida S/N, 4200-072 Porto, Portugal;
R. Henrique Portuguese Oncology Institute of Porto, Department of Pathology and Cancer Biology and Epigenetics Group-Research Centre, Rua Dr. António Bernardino de Almeida S/N, 4200-072 Porto, Portugal; Department of Pathology and Molecular Immunology, Institute of Biomedical Sciences Abel Salazar – University of Porto (ICBAS-UP), Rua de Jorge Viterbo Ferreira, 228, 4050-313 Porto, Portugal;
L. Oliveira Polytechnic of Porto, School of Engineering, Physics Department, Rua Dr. António Bernardino de Almeida, 431, 4200-072 Porto, Portugal; Centre of Innovation in Engineering and Industrial Technology, ISEP, Rua Dr. António Bernardino de Almeida, 431, 4200-072 Porto, Portugal; e-mail: lmo@isep.ipp.pt;
V.V. Tuchin Research-Educational Institute of Optics and Biophotonics, Saratov State University, ul. Astrakhanskaya 38, 410012 Saratov, Russia; Laboratory of Laser Diagnostics of Technical and Living Systems, Institute of Precision Mechanics and Control, Russian Academy of Sciences, ul. Rabochaya 24, 410028 Saratov, Russia; Interdisciplinary Laboratory of Biophotonics, Tomsk State University, prosp. Lenina 36, 634050 Tomsk, Russia

Received 19 September 2018; revision received 6 November 2018
Kvantovaya Elektronika **49** (1) 13–19 (2019)
Submitted in English

Steven Jacques' recent paper [17] published in 2013 presents also considerable data for various tissues and describes the common equations to fit the dependences of the scattering coefficient (μ_s) and the reduced scattering coefficient (μ'_s) on the wavelength λ:

$$\mu_s(\lambda) \text{ or } \mu'_s(\lambda) = a'\left[f_{Ray}\left(\frac{\lambda}{500\text{ nm}}\right)^{-4} + (1 - f_{Ray}) \times \left(\frac{\lambda}{500\text{ nm}}\right)^{-b_{Mie}}\right]. \quad (1)$$

The two terms in Eqn (1) describe the contributions of Rayleigh and Mie scattering to μ_s (or μ'_s), where f_{Ray} is the fraction of the Rayleigh scattering contribution and b_{Mie} characterises the mean size of the Mie scatterers. Since in Eqn (1) the wavelength is normalised to 500 nm, a' represents the μ_s (or μ'_s) value at that wavelength.

In general, both scattering coefficients exhibit a smooth decreasing behaviour from the ultraviolet to the near-IR (NIR) wavelengths. The wavelength dependence for the absorption coefficient (μ_a) is not usually described in the literature, since the contribution of many tissue components (myoglobin, haemoglobin, lipids, proteins, water, etc.) turn it unsmooth. We have to consider that biological tissues have internal heterogeneous composition [8] and their optical properties are in fact an average result of the contributions from all tissue components. The scattering anisotropy factor g presents an increasing behavior with wavelength for the visible-to-NIR wavelength range [17]. This behaviour is in general well fitted with an exponential equation, as described by Eqn (2) [10] or Eqn (3) [8]:

$$g(\lambda) = a + b\left[1 - \exp\left(\frac{\lambda - c}{d}\right)\right], \quad (2)$$

$$g(\lambda) = a\exp(b\lambda) - c\exp(-d\lambda). \quad (3)$$

The appropriate values for the parameters a, b, c and d are estimated when the data fitting is performed. The scattering coefficients and g are related through Eqn (4), meaning that if we have two of them, the calculation of the third one is possible [4, 10]:

$$\mu'_s(\lambda) = \mu_s(\lambda)[1 - g(\lambda)]. \quad (4)$$

Once these optical properties are estimated, they can be used to calculate others. One of very useful parameters is the light penetration depth [9, 13]:

$$\delta(\lambda) = \frac{1}{\sqrt{3\mu_a(\lambda)(\mu_a(\lambda) + \mu'_s(\lambda))}}. \quad (5)$$

The light penetration depth is necessary for accurate determination of the irradiation dose in photothermal and photodynamic therapy procedures of several diseases [4].

A no less important optical property of biological tissues is the RI. The RI can be measured experimentally and it also depends on the wavelength. Usually, the RI decreases with wavelength within the visible-to-NIR range. The common equations that are used to fit such wavelength dependence are the Cauchy equation (6), the Conrady equation (7) and the Cornu equation (8) [18, 19]:

$$n(\lambda) = A + \frac{B}{\lambda^2} + \frac{C}{\lambda^4}, \quad (6)$$

$$n(\lambda) = A + \frac{B}{\lambda} + \frac{C}{\lambda^{3.5}}, \quad (7)$$

$$n(\lambda) = A + \frac{B}{(\lambda - C)}. \quad (8)$$

The RI is in general measured at discrete laser wavelengths and then the experimental data is fitted with one of the previous equations. All these equations can be tested to see which one provides a better data fitting. When the best equation is selected and the fitting is made, the parameters A, B and C are estimated.

The human liver is a very important organ, since it metabolises drugs, detoxifies chemicals and filters blood coming from the digestive tract, before passing it to the rest of the body [20]. For human adults, liver contains a total of 74.5% of water and the remaining 25.5% are a combination of lipids, proteins, carbohydrates and minerals [21]. Roughly hexagonal units, designated as hepatic lobules, compose the liver. Each of these units is composed of liver parenchymal cells (hepatocytes), arranged into plates, lined by a vascular network of sinusoids that empty into a central vein, and a portal triad at the lobule's corners. Portal triads or portal tracts are structural element of the liver located at the vertices of the hepatic lobule, typically containing a branch of the hepatic artery, a branch of the portal vein and a bile duct. Figure 1 presents a typical histology section of human liver.

There are several diseases that can develop in liver, namely, hepatitis, cirrhosis and various forms of liver cancer [20, 22]. Due to the importance of liver functions and also since various pathologies can develop in this organ, its optical properties are of interest for clinical research, as demonstrated by some publications. Beauvoit et al. [23] studied the contribu-

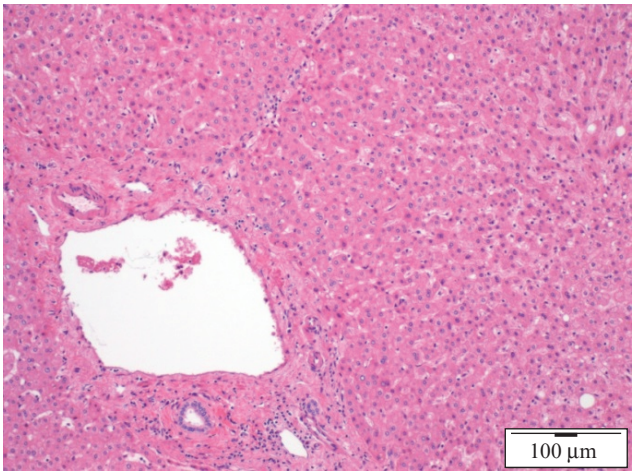

Figure 1. Human liver histology section, showing hepatocyte plates and a portal triad (lower left) (HE, 100×).

tion of mitochondria in the optical properties of rat liver at 780 nm, and Ritz et al. [24] compared the optical properties of normal and coagulated porcine liver. A study was also published where no significant variations are observed on the optical properties of rat liver at 830 nm when treated with some optical clearing agents (OCAs) [25].

With the objective of estimating the wavelength dependences of the optical properties of human liver between 400 and 1000 nm, we have performed some sets of optical measurements and IAD simulations.

2. Materials and methods

To estimate the optical properties of human liver from visible-to-NIR wavelength range, we have performed various optical measurements and used the IAD simulations. Subsection 2.1 describes the methodology used to collect and prepare the tissue samples. The procedure used for the RI measurements and liver dispersion estimation is presented in Sub-section 2.2, while the procedures used to obtain the spectral T_c, T_t and R_t measurements are described in Subsection 2.3. The estimation of the optical properties is described in Sub-section 2.4.

2.1. Sample collection and preparation

Five human adults, aged between 41 and 61, undergoing partial liver resection at the Portuguese Oncology Institute of Porto, Portugal, have signed a written consent previous to surgical interventions, allowing the subsequent use of surgical specimens for diagnostic and research purposes. The agreement has been approved by the Ethics Committee of the Portuguese Oncology Institute of Porto, Portugal.

Since surgeries usually occur during the afternoon, liver excisions were kept frozen at −80 °C for 16h before preparation to use in studies during the following day. Early in the morning of the day following surgery, samples were immersed in distilled water to defreeze and reach natural hydration.

Smaller liver samples were prepared from the liver resections with circular form of diameter 10 mm and thickness of 0.5 mm. A cryostat (CM 1850 UV Leica^{TM} model) was used to prepare these samples and the thickness precision was 10 μm. Distilled water was again used to freeze the samples, prior to slicing with the cryostat. A total of 30 samples were prepared with these dimensions to be used in the spectral measurements of T_c, T_t and R_t.

For the RI measurements, on the other hand, we prepared a total of 3 samples of rectangular shape (∼4 × 3 cm) and ∼1 cm thickness. These samples were flattened with the cryostat on one side to adhere perfectly to a prism surface during measurements with the total internal reflection method.

2.2. Estimation of liver dispersion

To estimate the dispersion of human liver between 400 and 1000 nm, we used the total internal reflection method [18, 19, 26–29]. The setup used to perform the measurements with various lasers at different wavelengths is presented in Fig. 2.

Each of the three samples was used to measure the RI at different laser wavelengths with the setup in Fig. 2. The laser wavelengths used in these measurements were 401.4, 532.5, 668.1, 782.1, 820.8 and 850.7 nm [30, 31]. A mean RI value for liver was obtained at each of these wavelengths [29, 30] and using CFTOOL from MATLAB^{TM}, Eqns (6–8) were tested to fit that data. The best fitting was obtained with the Cornu equation (8), where the R-square was 0.999. The calculated dispersion for human liver between 400 and 1000 nm is described by Eqn (9) [29].

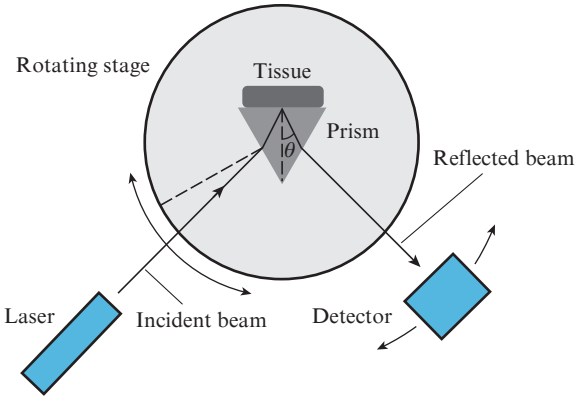

Figure 2. Setup used for RI measurements with the total internal reflection method.

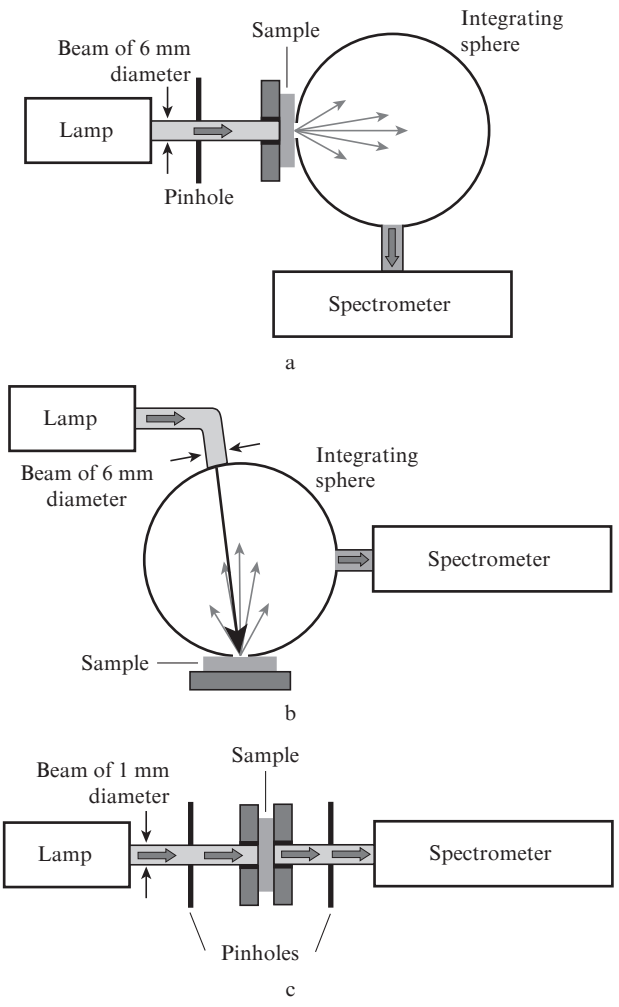

Figure 3. Setups for spectral measurements of (a) T_t, (b) R_t and (c) T_c.

$$n_{\text{liver}}(\lambda) = 1.3535 + \frac{13.56}{\lambda - 37.24}. \quad (9)$$

The RI values for the liver to be used in the IAD simulations were retrieved from this equation, as explained in Subsection 2.4.

2.3. Spectral optical measurements

As previously indicated, we used the IAD simulation code to estimate the wavelength dependences for the optical properties of human liver between 400 and 1000 nm. We needed to conduct optical spectral measurements of T_c, T_t and R_t from native liver samples in the same spectral range, since they are also needed in the simulations. For each of these measurements, 10 spectra were acquired from individual samples, so that a complete set of simulations could be done for each tissue sample and finally averaged to obtain statistical results. The setups used to perform these measurements are presented in Fig. 3. The mean spectra acquired with each of these setups are presented in Section 3.

2.4. Estimation of spectral optical properties of human liver

After acquiring all necessary experimental data, we estimated the optical properties of human liver, by performing several IAD simulations. Since each simulation is referred to a single wavelength, we had to select various wavelengths within the 400–1000 nm range to obtain good wavelength dependence for the optical properties of liver. Human liver contains a significant amount of blood, meaning that we need to obtain a good wavelength resolution near the absorption bands of myoglobin and haemoglobin. The wavelengths to perform the IAD simulations were selected at each 25 nm between 400 and 1000 nm. Additionally, between 400 and 600 nm, we selected other wavelengths separated by 10 nm.

Considering each of the 10 liver samples, we performed a set of IAD simulations, one for each of the selected wavelengths. The inputs for these simulations were the experimental T_c, T_t and R_t data at the corresponding wavelengths, the RI from Eqn (9) at the same wavelengths and the sample thickness of 0.5 mm. The outputs of the simulation are μ_a, μ'_s and g for the same wavelengths. Since g is not obtained with good precision from IAD simulations, we neglected this result. Instead, using the generated μ_a and sample thickness d, we calculated μ_s from the T_c measurements directly:

$$\mu_s = -\frac{\ln T_c}{d} - \mu_a. \quad (10)$$

Using μ'_s and μ_s in Eqn (4), we calculated g for each wavelength and for each sample. Finally, using μ'_s and μ_a data in Eqn (5), we also calculated δ for each wavelength and for each sample. After obtaining the wavelength dependences of all optical properties for each of the 10 samples, mean spectral optical properties between 400 and 1000 nm were calculated. The results are presented in Section 3.

3. Results

As a result of our previous RI study for human liver [29], the estimated dispersion curve [Eqn (9)] is presented in Fig. 4. The

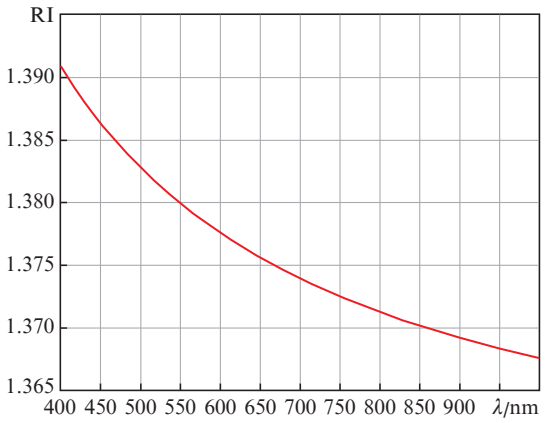

Figure 4. Wavelength dependence for the RI of human liver.

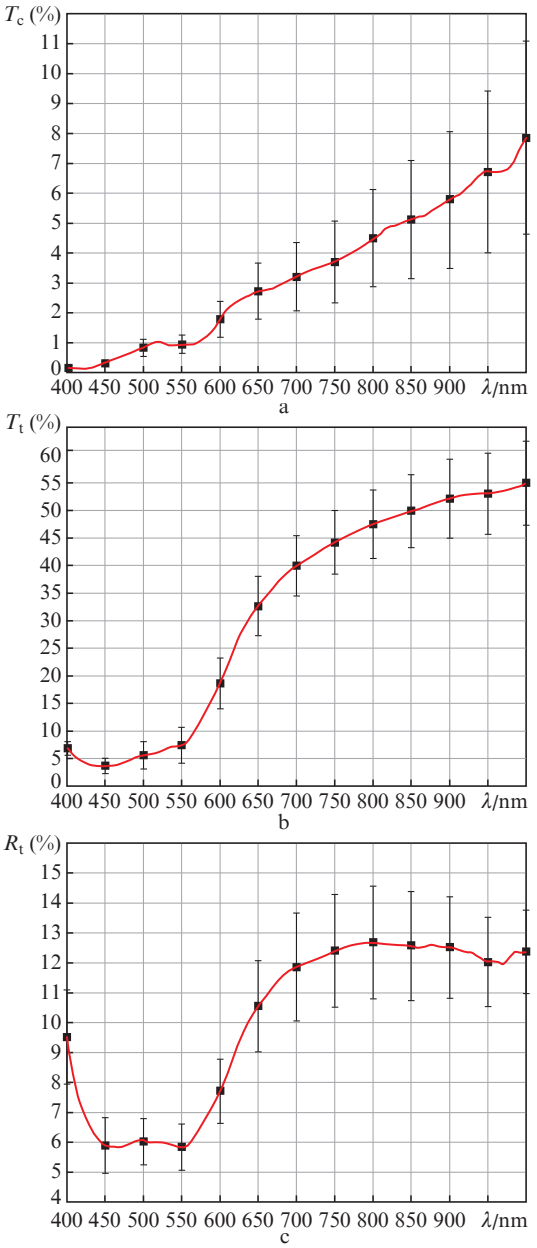

Figure 5. Mean spectra from human liver for (a) T_c, (b) T_t and (c) R_t.

RI values to be used in the IAD simulations were retrieved from this curve.

The spectral measurements obtained from all the 10 samples were averaged, so that Fig. 5 presents the statistical mean and standard deviation (SD) for T_c, T_t and R_t spectra of human liver.

All graphs in Fig. 5 have a wavelength resolution of 1 nm and the bars presented at each 50 nm represent the SD values calculated from the 10 measurements. These bars are only presented at each 50 nm for better visual perception. All graphs show the presence of blood in the studied liver samples. All the mean spectra represented in Fig. 5 show similar wavelength dependences similar to those obtained for other biological tissues, which can be found in the literature [9, 16].

Using the spectral data from each of the 10 individual samples we estimated the spectra for the optical properties of

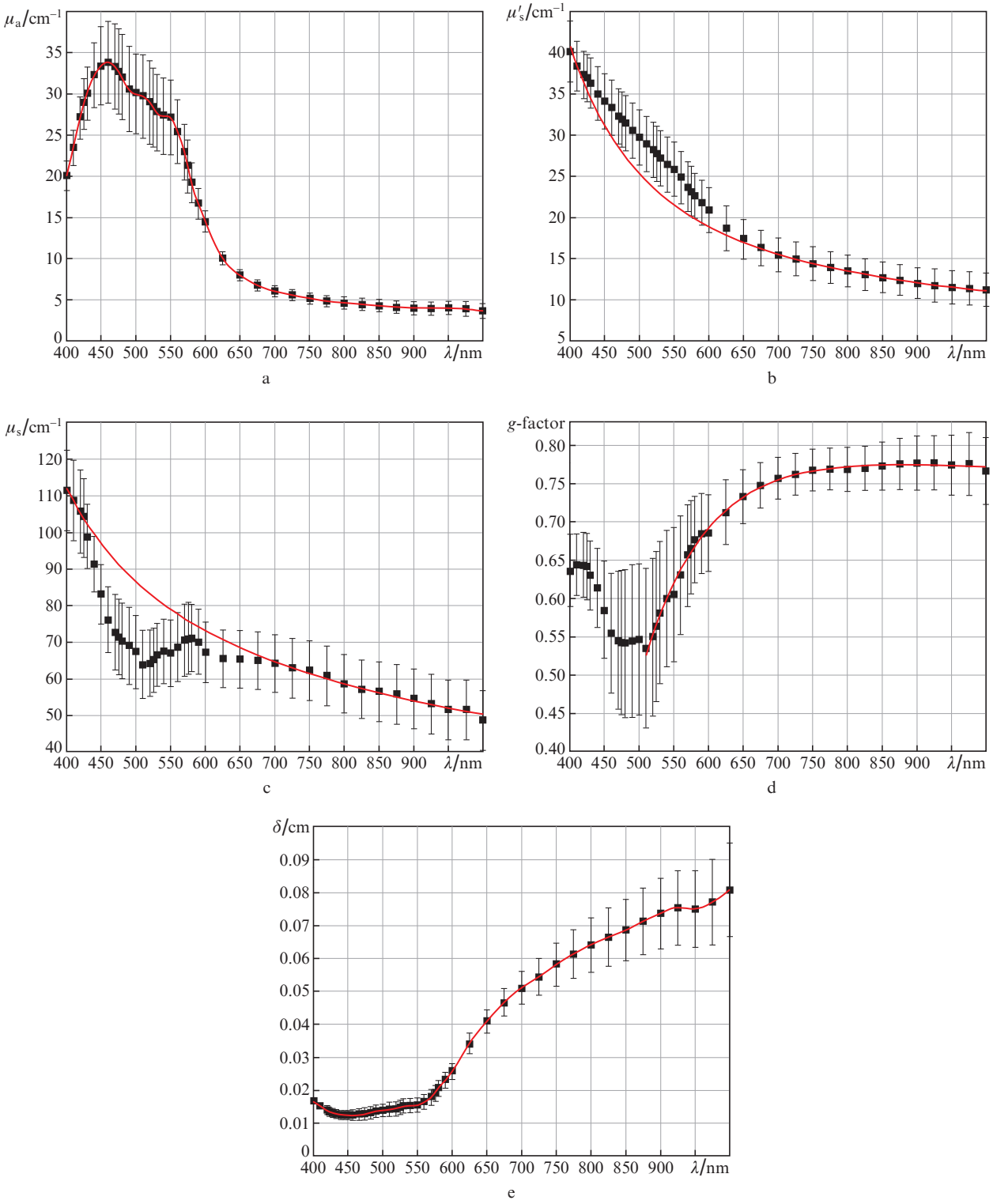

Figure 6. Mean optical properties [(a) μ_a, (b) μ'_s, (c) μ_s, (d) g and (e) δ] of human liver between 400 and 1000 nm.

human liver, through IAD simulations and calculations with Eqns (4), (5) and (10). The mean spectra for the optical properties of human liver, presented in Fig. 6, were calculated from the individual estimated/calculated results.

The estimated data points and the represented error bars in all graphs in Fig. 6 have the wavelength resolution indicated in Sub-section 2.4.

For the graph of μ_a presented in Fig. 6a, we have introduced a smooth spline to interpolate estimated data. The curve presented in the graph of Fig. 6b was calculated according to Eqn (1) to fit the μ'_s data:

$$\mu'_s(\lambda) \equiv 25.34\left[0.3537\left(\frac{\lambda}{500\ \text{nm}}\right)^{-4} + (1-0.3537) \times \left(\frac{\lambda}{500\ \text{nm}}\right)^{-0.6422}\right]. \quad (11)$$

The data fitting with Eqn (11) was obtained with an R-square value of 0.9999, by neglecting the estimated points between 420 and 625 nm. Equation (11) shows that the Rayleigh contribution is a little smaller than the Mie contribution, i.e. $f_{Ray} = 0.3537$.

A similar procedure was made to fit the μ_s data. The fitting curve presented in the graph of Fig. 6c was obtained by neglecting the estimated points between 430 and 650 nm, with an R-square value of 0.9985, and is described as:

$$\mu_s(\lambda) \equiv 86.55\left[0.112\left(\frac{\lambda}{500\ \text{nm}}\right)^{-4} + (1-0.112) \times \left(\frac{\lambda}{500\ \text{nm}}\right)^{-0.6317}\right]. \quad (12)$$

In this case, the Rayleigh contribution is significantly smaller than the Mie contribution, since $f_{Ray} = 0.112$.

For the case of $g(\lambda)$, the calculated data could be fitted with a curve described by Eqn (3), but only for wavelengths above 510 nm. The calculated fitting curve that is presented in Fig. 6d was obtained with an R-square value of 0.9947 and is described by:

$$g(\lambda) \equiv 0.8275\exp(-6.782\times10^{-5}\lambda) - 72.98\exp(-0.01095\lambda). \quad (13)$$

Finally, for the case of δ, we see a typical wavelength dependence [9] – low values of δ where absorption is high and increasing with wavelength where absorption decreases. The curve presented in the graph of Fig. 6e is a simple smooth spline that interpolates the calculated points. In that curve we see the water absorption band in the NIR range, with the peak near 950 nm [8]. The error bars in Fig. 6e result from the calculation with Eqn (5) and they show small values below 600 nm. These low values for the SD at low wavelengths indicate great similarity between the 10 samples studied in terms of bile and blood content.

From the data in the graphs of Fig. 6, we retrieved the values for the various optical properties of human liver at typical laser wavelengths. The data is presented in Table 1.

Table 1. Mean optical properties of human liver at laser wavelengths.

Laser	Wavelength/nm	μ_a /cm^{-1}	μ'_s /cm^{-1}	μ_s /cm^{-1}	g	δ /μm
He–Cd	441.6	32.5	32.42	99.09	0.6139	124,4
Ar^+	488	30.8	26.51	88.73	0.5445	134.9
He–Ne	632.8	9.18	17.56	70.00	0.7214	366
Ruby	694.3	6.16	15.67	65.06	0.7529	502.6
Nd:YAG	946	4.00	11.57	52.13	0.7738	750.6

4. Discussion

Figure 6a shows strong absorption for wavelengths below 600 nm and low absorption at higher wavelengths. This is a typical absorption spectrum for biological tissues [8, 9], resulting from the presence of blood, but the absorption peaks are not located at the expected wavelengths. It is well known that normal oxygenated blood presents three bands: at 415 nm (Soret band) and at 542 and 578 nm (Q-bands). Deoxygenated blood presents two bands at 425 and 554 nm [4]. For the case of rat liver, studies have showed the presence of deoxygenated blood at these wavelengths [32], and for native and coagulated porcine liver, peaks at these wavelengths were also found [24]. In our case, we obtained also three absorption peaks, but located at 460, 515 and 550 nm. This means that we are not seeing only blood in the liver samples. Some other chromophore in the liver samples that we used in our study shifted the absorption peaks. According to Ref. [33], bile is an endogenous compound which is abundant in liver. Bile has a specific absorption spectrum with a local minimum at 350 nm and local maxima at 409 and 605 nm [34]. The total absorption of tissue is described as the sum of the absorptions of the various tissue chromophores [34]:

$$\mu_a^{\text{Tissue}}(\lambda) = \mu_a^{\text{blood}}(\lambda) + \mu_a^{H_2O}(\lambda) + \mu_a^{\text{bile}}(\lambda) + \ldots, \quad (14)$$

where $\mu_a^{\text{blood}}(\lambda)$, $\mu_a^{H_2O}(\lambda)$ and $\mu_a^{\text{bile}}(\lambda)$ are the absorption spectra of blood, water and bile. For a typical biological tissue, other chromophores, like lipids, for example, might be present and the absorption spectrum of blood might have a combination of oxygenated and deoxygenated haemoglobin. Since we saw in Fig. 6a the occurrence of the three peaks at unexpected wavelengths between 400 and 600 nm, we might explain such peaks as a combination of oxygenated and deoxygenated blood with bile in specific quantities. The determination of the precise content for each of these chromophores would be possible with further studies and analysis. For wavelengths between 600 and 1000 nm, the values of μ_a decrease, showing a similar behavior to the one observed for tissue phantoms [35], or other biological tissues, such as colorectal tissues [8, 9]. The observed μ_a values for these longer wavelengths are similar to the ones observed for chicken and porcine liver [24, 36, 37]. The same evidence of a combination between bile and oxygenated/deoxygenated blood in the liver samples is also visible in the graphs of Fig. 6 for μ'_s, μ_s and g.

When fitting μ'_s, μ_s and g data, we neglected some points within particular wavelength ranges, as indicated in Section 3. Those neglected points that are not well fitted by typical equations within the entire range from 400 to 1000 nm indicate the presence of bile, oxygenated and deoxygenated blood in human liver samples. This evidence is not observed for

native porcine liver, since the published data [24] for this animal can be fitted with the typical curves in the entire range from 400 to 1000 nm.

For wavelengths longer than those where our data is not well fitted, the decreasing wavelength dependence observed for μ'_s and μ_s and the increasing wavelength dependence observed for g correspond to those that were observed for tissue phantoms [35], for other human tissues [8, 9], and also for animal [24, 37] or human liver [36], although the magnitude of the values is different.

The wavelength dependences for the optical properties of human liver between 400 and 1000 nm were not previously known. By performing this study, we could estimate those wavelength dependences and observe that in the case of human liver, the combination of some chromophores produces significant changes in those wavelength dependences for small wavelengths.

5. Conclusions

The estimation of the wavelength dependences of tissue's optical properties is highly necessary for the development of light propagation models and methods to be used in clinical diagnosis and treatment. Liver is a highly important organ in the human body and various pathologies are known to develop there, meaning that the estimation of its optical properties is of high interest. The estimated wavelength dependences for the optical properties of human liver allow for identification of liver properties at individual laser wavelengths which are used in diagnostics and treatment procedures. These results show that the absorption coefficient indicates the presence of oxy- and deoxy-haemoglobin and also of bile in the liver samples that were studied. Their combination leads to strong absorption for wavelengths below 600 nm and changes also the wavelength dependence of the other optical properties in this wavelength range. The absorption spectra of bile and oxy- and deoxy-haemoglobin can be used in future studies to estimate the content of these chromophores in liver samples.

The results presented for the natural liver can also be used as reference to evaluate the kinetics of the optical properties during optical clearing treatments to be applied to the liver. Using data measured during such treatments, we plan evaluate the kinetics for the refractive index, scattering coefficients and g.

We plan to conduct similar studies to estimate the wavelength dependence for the optical properties of other biological tissues in the near future.

Acknowledgements. This research was supported by the Portuguese research grant UID-EQU-04730-2013. Work of VVT was supported by the Russian Foundation for Basic Research (Grant No. 17-00-00275 (17-00-00272)].

References

1. Bucharskaya A. et al. *Int. J. Mol. Sci.*, **17** (8), E1295-1-26 (2016).
2. Bucharskaya A. et al. *Las. Surg. Med.* (2018); doi: 10.1002/lsm.23001.
3. Bashkatov A.N. et al. *Quantum Electron*, **44** (8), 779 (2014) [*Kvantovaya Elektron.*, **48** (8), 779 (2014)].
4. Tuchin V.V. *Tissue Optics: Light Scattering Methods and Instruments for Medical Diagnosis* (Bellingham: SPIE Press, 2015).
5. Vo-Dinh T. (Ed.) *Biomedical Photonics Handbook* (Boca Raton: CRC Press, 2014).
6. Wang L.-H. et al. *Comp. Method. Progr. Biomed.*, **47** (2), 131 (1995).
7. Prahl S.A. et al. *Appl. Opt.*, **32** (4), 559 (1993).
8. Carvalho S. et al. *Proc. SPIE*, **10063**, 100631L-1-16 (2017); doi:10.1117/12.2253023.
9. Carneiro I. et al. *Proc. SPIE*, **10685**, 106853D-1-12 (2018); doi:10.1117/12.2253023.
10. Bashkatov A.N. et al. *Opt. Spectrosc.*, **120** (1), 1 (2016) [*Opt. Spektrosk.*, **120** (1), 6 (2016)].
11. https://omlc.org/software/.
12. Firbank M. et al. *Phys. Med. Biol.*, **38** (4), 503 (1993).
13. Bashkatov A.N. et al. *J. Phys. D: Appl. Phys.*, **38** (15), 2543 (2005).
14. Tromberg B.J. et al. *Phil. Trans. R. Soc. Lond. B*, **352** (1354), 661 (1997).
15. Matcher S.J. et al. *Appl. Opt.*, **36** (1), 386 (1997).
16. Bashkatov A.N. et al. *Med. Las. Applicat.*, **22** (2), 95 (2007).
17. Jacques S.L. *Phys. Med. Biol.*, **58** (11), R37 (2013).
18. Ding H. et al. *Phys. Med. Biol.*, **51** (6), 1479 (2006).
19. Deng Z. et al. *J. Biomed. Opt.*, **21** (1), 015003 (2016).
20. Armuzzi A. et al. *Aliment. Pharmacol. Ther.*, **16** (12), 1977 (2002).
21. White D.R. et al. *Br. J. Radiol.*, **64** (758), 149 (1991).
22. Liver Cancer Study Group of Japan. *Japn. J. Surg.*, **19** (1), 98 (1989).
23. Beauvoit B. et al. *Biophys. J.*, **67** (6), 2501 (1994).
24. Ritz J.-P. et al. *Las. Surg. Med.*, **29** (3), 205 (2001).
25. Liu H. et al. *J. Biomed. Opt.*, **1** (2), 200 (1996).
26. Li H., Xie S. *Appl. Opt.*, **35** (10), 1793 (1996).
27. Ding H. et al. *J. Opt. Soc. Am. A*, **22** (6), 1151 (2005).
28. Jin Y.L. et al. *Phys. Med. Biol.*, **51** (20), N271 (2006).
29. Carneiro I. et al. *J. Biomed. Opt.*, **22** (12), 125002-1-10 (2017).
30. Carneiro I. et al. *J. Biomed. Phot. Eng.*, **3** (4), 040301-1-10 (2017).
31. Carvalho S. et al. *J. Biomed. Phot. Eng.*, **2** (4), 040307-1-9 (2016).
32. Parsa P. et al. *Appl. Opt.*, **28** (12), 2325 (1989).
33. Maitland D.J. et al. *Appl. Opt.*, **32** (4), 586 (1993).
34. Nachabé R. et al. *Biomed. Opt. Express*, **2** (3), 601 (2011).
35. Wróbel M.S. et al. *Biomed. Opt. Express*, **7** (6), 2088 (2016).
36. Germer C.-T. et al. *Las. Surg. Med.*, **23**, 194 (1998).
37. Hafeez-Ullah et al. *Opt. Spectrosc.*, **110** (2), 313 (2011).